J. Fluid Mech. (1996), *vol.* 325, *pp.* 29–51

The linear stability of mixed convection in a vertical channel flow

By YEN-CHO CHEN[1] AND J. N. CHUNG[2]

[1] Oriental Institute of Technology, Panchiao, Taiwan, R.O.C.

[2] School of Mechanical and Materials Engineering, Washington State University, Pullman, WA 99164-2920, USA

(Received 26 April 1994 and in revised form 22 March 1996)

In this study, the linear stability of mixed-convection flow in a vertical channel is investigated for both buoyancy-assisted and -opposed conditions. The disturbance momentum and energy equations were solved by the Galerkin method. In addition to the case with a zero heat flux perturbation boundary condition, we also examined the zero temperature perturbation boundary condition. In general, the mixed-convection flow is strongly destabilized by the heat transfer and therefore the fully developed heated flow is very unstable and very difficult to maintain in nature. For buoyancy-assisted flow, the two-dimensional disturbances dominate, while for buoyancy-opposed flow, the Rayleigh–Taylor instability prevails for zero heat flux perturbation boundary condition, and for the zero temperature perturbation on the boundaries the two-dimensional disturbances dominate except at lower Reynolds numbers where the Rayleigh–Taylor instability dominates again. The instability characteristics of buoyancy-assisted flow are found to be strongly dependent on the Prandtl number whereas the Prandtl number is a weak parameter for buoyancy-opposed flow. Also the least-stable disturbances are nearly one-dimensional for liquids and heavy oils at high Reynolds numbers in buoyancy-assisted flows.

From an energy budget analysis, we found that the thermal–buoyant instability is the dominant type for buoyancy-assisted flow. In buoyancy-opposed flow, under the zero temperature perturbation boundary condition the Rayleigh–Taylor instability dominates for low-Reynolds-number flow and then the thermal–shear instability takes over for the higher Reynolds numbers whereas the Rayleigh–Taylor instability dominates solely for the zero heat flux perturbation boundary condition. It is found that the instability characteristics for some cases of channel flow in this study are significantly different from previous results for heated annulus and pipe flows. Based on the distinctly different wave speed characteristics and disturbance amplification rates, we offer some suggestions regarding the totally different laminar–turbulent transition patterns for buoyancy-assisted and -opposed flows.

1. Introduction

In engineering applications, most flow are non-isothermal. Mixed convection in vertical channels, tubes and ducts has been extensively investigated because of its applications to nuclear reactors, heat exchangers, electronic equipment and other areas of practical interests. In engineering, the assumption of a fully developed flow is often used to simplify the governing partial differential equations of a laminar flow such that ordinary differential equations result. Thus an analytic solution of the laminar flow is obtained and the characteristics of fluid flow and heat transfer can be easily analysed.

But the flows that occur in nature must not only obey those simplified fluid dynamics and heat transfer equations, but also must be stable in order to be represented by the simple fully developed flow solutions, otherwise different forms of convective flow will occur because of the flow instability and transition.

Many previously published research results seem to indicate that non-isothermal flow instability and transition differ substantially from those of an isothermal flow (Gebhart *et al.* 1988; Yao 1987*a*, *b*). For example, at low Reynolds numbers mixed-convection pipe flows frequently become unstable even under mild heating conditions (Scheele & Hanratty 1962; Kemeny & Somers 1962). The experimental results by Hanratty, Rosen & Kabel (1958), Scheele, Rosen & Hanratty (1960) and Kemeny & Somers (1962) all showed that heated vertical pipe flow can go through a flow transition at a Reynolds number as low as 30. Scheele & Hanratty (1962) observed that during the low-Reynolds-number flow transition the flow consisted mainly of large-scale, regular and periodic motions which were confirmed by Yao (1987*a*, *b*) in a linear stability analysis. Yao found that the unstable flow is a double-spiral with wavelengths comparable to the pipe diameter and the motion is regular and periodic. Scheele & Hanratty (1962) also found that the temperature fluctuations of such low-Reynolds-number flows of water during transition in a vertical heated pipe are low-frequency and small-scale oscillations. Kemeny & Somers (1962) called such a very low-Reynolds-number transition flow 'non-laminar flow' to distinguish it from the turbulent flow and found that the Nusselt numbers of non-laminar flows can be 30% higher than those of laminar flow. A significant increase of the Nusselt number above those of laminar flows during low-Reynolds-number flow transition was also observed by Maitra & Raju (1975) in the mixed-convection flow of a heated vertical annulus.

Sheele & Hanratty (1962) also noted that for heated upflow (buoyancy assisted) in a pipe the flow first becomes unstable when the velocity profiles develop points of inflection. Transition to an unsteady flow involves the gradual growth of small disturbances and therefore it is quite possible to have unstable flows without observing transition when the pipe is not long enough. For heated downflow (buoyancy opposed), transition to an unsteady flow is sudden and therefore transition occurs shortly after an unstable flow occurs. The experimental observation of Sheele & Hanratty (1962) was confirmed by a weakly nonlinear instability analysis of Rogers & Yao (1993*a*) who found that heated upflow is supercritically unstable while heated downflow is potentially subcritically unstable. Furthermore, Sheele & Hanratty (1962) observed in their experiment that the stability depends primarily on the shape of the velocity profile which is modified by the heating and only secondarily depends on the Reynolds number, if at all. Recently, El-Genk & Rao (1990) reported some experimental results for buoyancy-induced instability in a vertical annulus for low-Reynolds-number flows. They found phenomena similar to those in a pipe. They stated that in buoyancy-assisted flow, three successive regions of stable laminar, local flow mixing and turbulent flows were observed, which indicates that the transition is gradual and represents a supercritically unstable flow. For buoyancy-opposed flow, the flow field consists of only stable laminar and turbulent regions, which means the transition is abrupt and the flow is subcritically unstable.

The first theoretical work on this topic was reported by Yao (1987*a*, *b*), who performed a linear stability analysis for heated vertical pipe flow of water and found that the fully developed non-isothermal flow is highly unstable. The flow can become unstable when both the Rayleigh number > 75 and the Reynolds number > 40. The most unstable azimuthal wavenumber is unity. Yao and his associates have also recently reported important work on identifying linear thermal instabilities in a vertical

annulus (Yao & Rogers 1989*a*, *b*, 1992; Rogers & Yao 1993*b*; Rogers, Moulic & Yao 1993) and in a vertical pipe (Rogers & Yao 1993*a*). Basically there are two sources of the thermal instabilities – shear production and thermal buoyant potential. For stably stratified flows with constant heat flux imposed on the wall, the type of instability is strongly depend on the Prandtl number. In the first type, which was found primarily for lower-Prandtl-number fluids, the instability is initiated when the basic-state velocity profile is distorted sufficiently to become unstable as a result of increased Rayleigh number or heating, but most of the kinetic energy for the instability comes from the shear production. They termed this category of flow *thermal–shear instability*. The second thermal instability, which dominates in higher-Prandtl-number fluids, obtains its kinetic energy primarily from thermal buoyant potential. This type is called *thermal–buoyant instability*. The thermal–buoyant instability is driven by buoyancy forces due to heating and is more sensitive to thermal effects as a disturbance of the buoyant force, induced by a temperature fluctuation, causes a disruption in the velocity field. The reason that the lower-Prandtl-number fluids do not exhibit thermal–buoyant instability is the lack of temperature fluctuations. In lower-Prandtl-number fluids, the temperature fluctuations are rapidly smoothed by conduction. For unstably stratified flows, the well-known *Rayleigh–Taylor* instability is dominant. Only at very large Prandtl number (~ 100) would the thermal–buoyant mode become active. At high Reynolds numbers, the shear instability prevails in annulus flow.

The theoretical analyses of linear stability in isothermal channel flow have been well documented (Drazin & Reid 1981). The well-known results for the critical Reynolds number $Re_c = 5772.22$ (based on the half-width of the channel and the maximum velocity) and wavenumber $\alpha_c = 1.02056$ are provided by Orszag (1971), while isothermal pipe flow is absolutely stable for any infinitesimal disturbance. On the other hand, fully developed laminar flow of mixed convection in a vertical channel with a constant vertical temperature gradient imposed on walls was studied by Ostrach (1954) and Tao (1960), but the stability of this flow has not been investigated and reported in the open literature. Since the instability characteristics of heated channel flow are related to the understanding of transition and turbulence, in this paper we investigate those characteristics of mixed convection in a vertical channel flow.

2. Formation

The viscous flow investigated in this paper is mixed convection, which is driven by an external pressure gradient and also by a buoyancy force, between two parallel long vertical plates separated by a distance $2d$. At the laminar state a constant heat flux condition is imposed on the walls and the heating level is identical for both walls. The gravitational force is aligned in the negative x-direction. A schematic of this system is given in figure 1. The dimensionless governing equations for continuity, momentum and energy can be written as

$$\nabla \cdot V = 0, \tag{1}$$

$$\frac{\partial V}{\partial t} + V \cdot \nabla V = -\nabla P + \frac{1}{Re}\nabla^2 V + \frac{Ra}{Re}\theta e_x, \tag{2}$$

$$\frac{\partial \theta}{\partial t} + V \cdot \nabla \theta = \frac{1}{Re\,Pr}(\nabla^2 \theta - u), \tag{3}$$

where the coordinates are non-dimensionalized by the half-width of the channel d, the velocity (V) by the mean laminar base velocity $\bar{U}_B$, the pressure (P) by $\rho \bar{U}_B^2$, and the

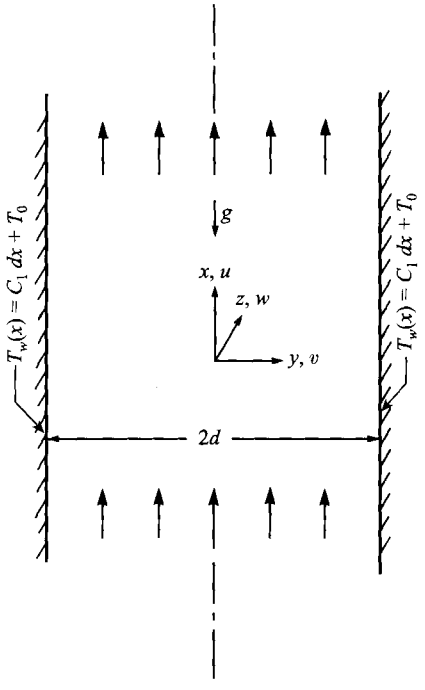

FIGURE 1. Schematic of the geometry and coordinate system.

time (t) by $d/\bar{U}_B$. Also, ρ is the fluid density, $\boldsymbol{e}_x$ is the unit vector in the x-direction, and (u, v, w) are the dimensionless velocity components in the streamwise (x), cross-streamwise (y, perpendicular to the walls) and spanwise (z) directions, respectively. In the above, $Re = \bar{U}_B d/\nu$ is the Reynolds number, where ν is the fluid kinematic viscosity, and $Pr = \nu/\alpha$ is the Prandtl number, where α is the thermal diffusivity. For a constant heat flux at the walls, Tao (1960) showed that the channel wall temperature increases or decreases linearly with x as $T_w(x) = T_0 + C_1 dx$, where C_1 is a constant and T_0 is the upstream reference wall temperature. C_1 is positive for buoyancy-assisted flow and negative for buoyancy-opposed flow. $Ra = g\beta C_1 d^4/\nu\alpha$ is the Rayleigh number, where g is the gravitational acceleration and β is the thermal expansion coefficient; it is positive for buoyancy-assisted flow and is negative for buoyancy-opposed flow. The Boussinesq approximation is used here. $\theta = (T - T_w)/C_1 d\, Re\, Pr$ is the dimensionless temperature, T being the instantaneous fluid temperature.

2.1. *Mean base flow*

The base flow is fully developed steady laminar flow, that is, it is a function of y only. By applying those assumptions, the above governing equations (2) and (3) can be reduced to

$$\frac{dP_B}{dx} = \frac{Ra}{Re}\theta_B + \frac{1}{Re}\frac{d^2U_B}{dy^2}, \tag{4}$$

$$\frac{d^2\theta_B}{dy^2} = U_B. \tag{5}$$

The associated boundary conditions are

$$U_B = \theta_B = 0 \quad \text{at} \quad y = \pm 1. \tag{6}$$

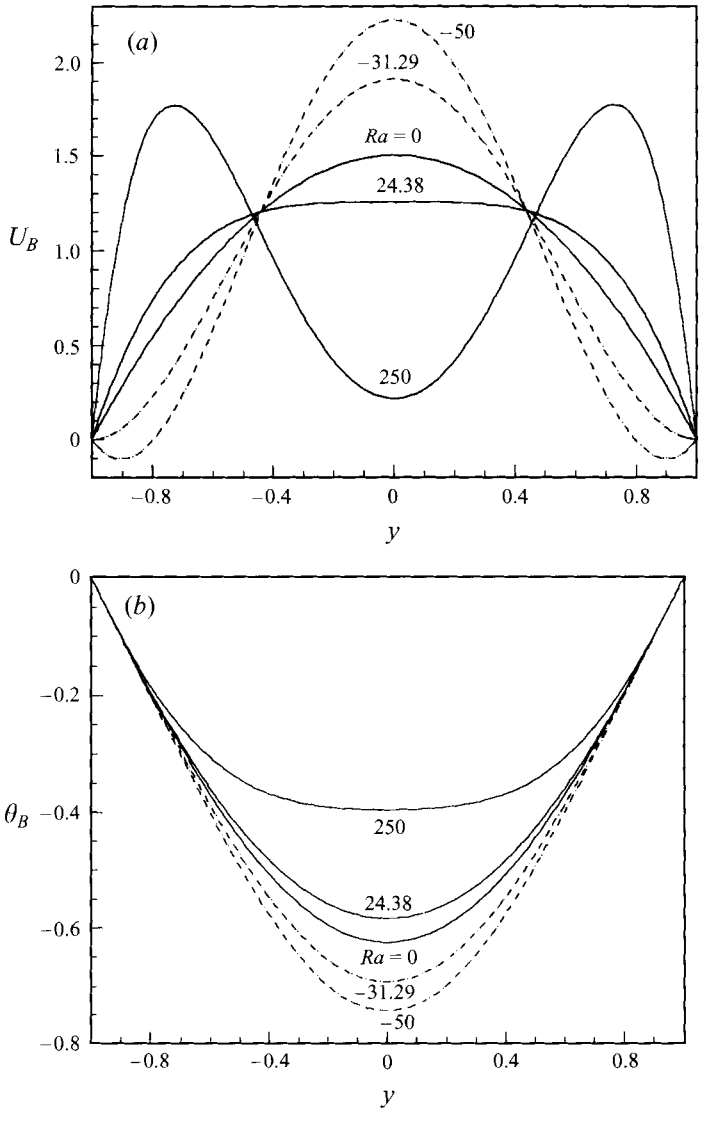

FIGURE 2. Laminar base profiles: (*a*) velocity, (*b*) temperature.

The solutions of (4)–(6) for buoyancy-assisted flow are (Tao 1960)

$$U_B = -\frac{E}{Ra^{1/2}} \frac{\sinh k(1+y)\sin k(1-y) + \sin k(1+y)\sinh k(1-y)}{\cosh 2k + \cos 2k}, \tag{7a}$$

$$\theta_B = \frac{E}{Ra}\left[1 - \frac{\cosh k(1+y)\cos k(1-y) + \cos k(1+y)\cosh k(1-y)}{\cosh 2k + \cos 2k}\right], \tag{7b}$$

and E is related to the pressure gradient:

$$E = Re\frac{\mathrm{d}P_B}{\mathrm{d}x} = -2k\,Ra^{1/2}(\cosh 2k + \cos 2k)/(\sinh 2k - \sin 2k). \tag{7c}$$

The solutions of (4)–(6) for buoyancy-opposed flow are (Hanratty *et al.* 1958)

$$U_B = \frac{F}{2m^2}\left(\frac{\cosh my}{\cosh m} - \frac{\cos my}{\cos m}\right), \quad \theta_B = \frac{F}{2m^4}\left(\frac{\cosh my}{\cos m} + \frac{\cos my}{\cos m} - 2\right), \tag{8a, b}$$

and F is related to the pressure gradient:

$$F = Re\frac{dP_B}{dx} = \frac{2m^3}{\tanh m - \tan m}, \tag{8c}$$

where $k = Ra^{1/4}/\sqrt{2}$ and $m = (-Ra)^{1/4}$. The only parameter in (7) and (8) is Ra. The laminar base-flow velocity and temperature profiles for $Ra = -50$, -31.29, 0, 24.38 and 250 are plotted in figures 2(*a*) and 2(*b*), respectively. The velocity profile starts to show inflection points when $Ra \geqslant 24.38$ and the inflection points move towards the walls as the Rayleigh number increases for buoyancy-assisted flow. For $|Ra| \geqslant 6.09$ in buoyancy-opposed flow, the velocity profile has points of inflection near the walls and the inflection points move towards the centre of the channel as the magnitude of the Rayleigh number ($|Ra|$) increases. At $|Ra| = 31.29$, the velocity gradients at the walls become zero and reversals of flow occur near the walls for further increase of the Rayleigh number magnitude.

2.2. *Linear stability analysis*

In the linear stability analysis, infinitesimal disturbances are imposed on the fully developed laminar base flow; thus the velocity, pressure and temperature fields can be written as

$$V = U_B(y)\,\boldsymbol{e}_x + V', \quad P = P_B(x) + p', \quad \theta = \theta_B(y) + \theta', \tag{9a–c}$$

where the prime denotes an infinitesimal disturbance. $V' = (u', v', w')$ where u', v' and w' are the velocity disturbances in x-, y-, and z-directions, respectively. By substituting equation (9) into (1)–(3) and neglecting the higher-order terms, the linearized continuity, momentum and energy equations for the perturbed quantities become

$$\nabla \cdot V' = 0, \tag{10}$$

$$\frac{\partial V'}{\partial t} + V' \cdot \nabla U_B + U_B \cdot \nabla V' = -\nabla p' + \frac{1}{Re}\nabla^2 V' + \frac{Ra}{Re}\theta' \boldsymbol{e}_x, \tag{11}$$

$$\frac{\partial \theta'}{\partial t} + U_B\frac{\partial \theta'}{\partial x} + v'\frac{d\theta_B}{dy} = \frac{1}{Re\,Pr}(\nabla^2\theta' - u'), \tag{12}$$

where $U_B = U_B(y)\,\boldsymbol{e}_x$. By using the usual normal mode form, the disturbances can be represented by

$$V' = \hat{V}(y)\,e^{i(\alpha x + \beta z - \alpha c t)}, \quad p' = \hat{p}(y)\,e^{i(\alpha x + \beta z - \alpha c t)}, \quad \theta' = \hat{\theta}(y)\,e^{i(\alpha x + \beta z - \alpha c t)}, \tag{13a–c}$$

where $\hat{V} = (\hat{u}, \hat{v}, \hat{w})$ with $\hat{u}$, $\hat{v}$ and $\hat{w}$ are the velocity components in the x-, y- and z-directions, respectively; α (real) and β (real) are the wavenumbers in the x- and z-directions, respectively; $c = c_r + ic_i$ is the complex wave speed. The growth or decay of the disturbance depends on c_i. The flow is stable, neutrally stable or unstable for $c_i < 0$, $c_i = 0$ or $c_i > 0$, respectively. By substituting equation (13) into (10)–(12) and eliminating the pressure terms, the linearized stability equations become

$$\frac{1}{Re}\left[\frac{\mathrm{d}^4\hat{v}}{\mathrm{d}y^4}-2(\alpha^2+\beta^2)\frac{\mathrm{d}^2\hat{v}}{\mathrm{d}y^2}+(\alpha^2+\beta^2)^2\hat{v}\right]+\mathrm{i}\alpha\left\{U_B\left[-\frac{\mathrm{d}^2\hat{v}}{\mathrm{d}y^2}+(\alpha^2+\beta^2)\hat{v}\right]+\frac{\mathrm{d}^2U_B}{\mathrm{d}y^2}\hat{v}\right\}$$
$$-\mathrm{i}\alpha\frac{Ra}{Re}\frac{\mathrm{d}\hat{\theta}}{\mathrm{d}y}=-\mathrm{i}\alpha c\left[\frac{\mathrm{d}^2\hat{v}}{\mathrm{d}y^2}-(\alpha^2+\beta^2)\hat{v}\right], \quad (14)$$

$$-\frac{1}{Re}\left[\frac{\mathrm{d}^2\hat{\eta}}{\mathrm{d}y^2}-(\alpha^2+\beta^2)\hat{\eta}\right]+\mathrm{i}\alpha U_B\hat{\eta}+\beta\frac{\mathrm{d}U_B}{\mathrm{d}y}\hat{v}-\beta\frac{Ra}{Re}\hat{\theta}=\mathrm{i}\alpha c\hat{\eta}, \quad (15)$$

$$-\frac{1}{Re\,Pr}\left[\frac{\mathrm{d}^2\hat{\theta}}{\mathrm{d}y^2}-(\alpha^2+\beta^2)\hat{\theta}\right]+\frac{1}{(\alpha^2+\beta^2)\,Re\,Pr}\left(\mathrm{i}\alpha\frac{\mathrm{d}\hat{v}}{\mathrm{d}y}+\beta\hat{\eta}\right)+\frac{\mathrm{d}\theta_B}{\mathrm{d}y}\hat{v}+\mathrm{i}\alpha U_B\hat{\theta}=\mathrm{i}\alpha c\hat{\theta}, \quad (16)$$

where $\hat{\eta}=\beta\hat{u}-\alpha\hat{w}$. The associated boundary conditions for non-permeable rigid walls with a constant heat flux are

$$\hat{v}=\frac{\mathrm{d}\hat{v}}{\mathrm{d}y}=\hat{\eta}=\frac{\mathrm{d}\hat{\theta}}{\mathrm{d}y}=0 \quad \text{at} \quad y=\pm 1. \quad (17)$$

Equations (14)–(16) and the corresponding boundary conditions constitute an eigenvalue problem.

2.3. *Numerical method*

The Galerkin method is used to solve the above coupled equations (14)–(16) and their associated boundary conditions. In this method, the test (weighted) functions are the same as the base (trial) functions. Thus $\hat{v}$, $\hat{\eta}$ and $\hat{\theta}$ are expanded as

$$\hat{v}=\sum_{n=0}^{N}a_n\xi_n(y), \quad \hat{\eta}=\sum_{n=0}^{N}b_n\zeta_n(y), \quad \hat{\theta}=\sum_{n=0}^{N}d_n\phi_n(y). \quad (18a\text{–}c)$$

We adopt the base function proposed by Singer, Ferziger & Reed (1989) for $\hat{v}$. The base functions for $\hat{\eta}$ and $\hat{\theta}$ have different forms in order to satisfy their respective boundary conditions. They are

$$\xi_n(y)=(1-y^2)^2P_n(y), \quad \zeta_n(y)=(1-y^2)P_n(y), \quad (18d, e)$$

$$\phi_n(y)=\begin{cases}(1-y^2)P_n(y)+2P_1, & n=\text{odd}\\ (1-y^2)P_n(y)+\frac{2}{3}P_2, & n=\text{even}.\end{cases} \quad (18f)$$

The base function $\phi_n(y)$ given in equation (18f) which satisfies the zero-heat-flux perturbation boundary condition specified in (17) is also non-zero at the boundaries. In other words, (18f) results in a non-zero temperature perturbation at the bounding walls. However, for a special case where the walls which bound the fluid have a higher thermal conductivity and a larger heat capacity than those of the fluid, Sparrow, Goldstein & Jonsson (1964) and Busse (1981) both suggest that the temperature perturbation of the fluid at the bounding walls is essentially zero. That is, $\hat{\theta}$ can be assumed zero at the boundaries with highly conducting walls. In practice, such a system can be realized for air, water or oil under heating or cooling in a channel or pipe with walls made of thick highly conducting metal such as copper. For this special case, the base function for ϕ_n may be chosen as

$$\phi_n(y)=(1-y^2)P_n(y). \quad (18g)$$

In (18), each of the base functions ξ_n, ζ_n and ϕ_n satisfies the boundary conditions and

$P_n(y)$ is the Legendre polynomial of order n. Multiplying equations (14)–(16) by test functions ξ_m, ζ_m and ϕ_m, respectively, and integrating across the channel yields

$$\frac{1}{Re}\sum_{n=0}^{N} a_n \int_{-1}^{1} [\xi_m'' \xi_n'' + 2(\alpha^2+\beta^2)\xi_m' \xi_n' + (\alpha^2+\beta^2)^2 \xi_m \xi_n]\,\mathrm{d}y$$
$$+ \mathrm{i}\alpha \sum_{n=0}^{N} a_n \int_{-1}^{1} \left\{\left[\frac{\mathrm{d}^2 U_B}{\mathrm{d}y^2} + (\alpha^2+\beta^2) U_B\right]\xi_m \xi_n - U_B \xi_m \xi_n''\right\}\mathrm{d}y - \mathrm{i}\alpha \frac{Ra}{Re}\sum_{n=0}^{N} d_n \int_{-1}^{1} \xi_m \phi_n'\,\mathrm{d}y$$
$$= \mathrm{i}\alpha c \sum_{n=0}^{N} a_n \int_{-1}^{1} [(\alpha^2+\beta^2)\xi_m \xi_n + \xi_m' \xi_n']\,\mathrm{d}y, \quad (19)$$

$$-\beta \sum_{n=0}^{N} a_n \int_{-1}^{1} [U_B(\zeta_m' \xi_n + \zeta_m \xi_n')]\,\mathrm{d}y + \frac{1}{Re}\sum_{n=0}^{N} b_n \int_{-1}^{1} [(\alpha^2+\beta^2)\zeta_m \zeta_n + \zeta_m' \zeta_n']\,\mathrm{d}y$$
$$+ \mathrm{i}\alpha \sum_{n=0}^{N} b_n \int_{-1}^{1} U_B \zeta_m \zeta_n\,\mathrm{d}y - \beta \frac{Ra}{Re}\sum_{n=0}^{N} d_n \int_{-1}^{1} \zeta_m \phi_n\,\mathrm{d}y = \mathrm{i}\alpha c \sum_{n=0}^{N} b_n \int_{-1}^{1} \zeta_m \zeta_n\,\mathrm{d}y, \quad (20)$$

$$-\sum_{n=0}^{N} a_n \int_{-1}^{1} [\theta_B(\phi_m' \xi_n + \phi_m \xi_n')]\,\mathrm{d}y + \frac{\mathrm{i}\alpha}{(\alpha^2+\beta^2) Re\, Pr}\sum_{n=0}^{N} a_n \int_{-1}^{1} \phi_m \xi_n'\,\mathrm{d}y$$
$$+ \frac{\beta}{(\alpha^2+\beta^2) Re\, Pr}\sum_{n=0}^{N} b_n \int_{-1}^{1} \phi_m \zeta_n\,\mathrm{d}y + \frac{1}{Re\, Pr}\sum_{n=0}^{N} d_n \int_{-1}^{1} [(\alpha^2+\beta^2)\phi_m \phi_n + \phi_m' \phi_n']\,\mathrm{d}y$$
$$+ \mathrm{i}\alpha \sum_{n=0}^{N} d_n \int_{-1}^{1} U_B \phi_m \phi_n\,\mathrm{d}y = \mathrm{i}\alpha c \sum_{n=0}^{N} d_n \int_{-1}^{1} \phi_m \phi_n\,\mathrm{d}y. \quad (21)$$

In (19)–(21), a prime on ξ or ζ denotes differentiation with respect to y. The integrations are evaluated either by the orthogonality properties of Legendre polynomials or by Lobatto quadrature (Davis & Rabinowitz 1984). The above coupled equations can be solved by the 'GVLCG' or 'GVCCG' subroutine in the IMSL Library. Before the code was used for the thermal instability study, we wanted to make sure, as far as possible, that it was verified. There are no experimental or analytical results for heated channel flow in the open literature to compare with our predictions, so we had to compare with published results for isothermal channel flow for $Ra \to 0^+$ and $Ra \to 0^-$ for buoyancy-assisted and buoyancy-opposed flows, respectively. Our isothermal results of $Re = 5772.22$, $\alpha = 1.02056$ and $Re = 10000$, $\alpha = 1$ (based on the maximum velocity and half-width) with $N = 51$ in equation (18) agree with those of Orszag (1971) to the fifth decimal point. $N = 51$ is therefore used in the current linear stability computation. It is noted that the Reynolds number in the current study is based on the mean velocity of the laminar flow while the centreline velocity was adopted in Orszag (1971). This is why the Re_c is 3848.147 in table 1 in §3.1 instead of the well-known 5772.22 given in Orszag (1971).

2.4. *Energy budget analysis*

In order to understand the role played by heat transfer during the flow instability, it is necessary to keep track of the turbulent kinetic energy budget for the disturbances. The driving mechanisms of flow instability may be determined by the production and dissipation of disturbance kinetic energy (Hart 1971; Rogers & Yao 1993*b*). The balance of disturbance kinetic energy for an infinitesimal disturbance is

$$\frac{\partial}{\partial t}\langle \tfrac{1}{2}(u'^2+v'^2+w'^2)\rangle = -\left\langle u'v'\frac{\mathrm{d}U_B}{\mathrm{d}y}\right\rangle + \frac{Ra}{Re}\langle u'\theta'\rangle - \frac{1}{Re}\langle (\nabla u')^2 + (\nabla v')^2 + (\nabla w')^2\rangle$$
$$= E_s + E_b + E_d, \quad (22)$$

where the angle bracket $\langle\ \rangle$ implies integration over the volume of the disturbance wave. The first term on the right-hand side of (22), E_s, represents the shear production of turbulent energy which is the product of the Reynolds stress and the mean flow strain rate. This shear production is identical to that in isothermal flow. The second term, E_b, represents the turbulent kinetic energy production due to the work done by the thermal buoyant potential of the disturbance temperature field. Therefore the contribution to the turbulent disturbance kinetic energy from heat transfer is represented by this term. The second term is thus absent in isothermal flow. The last term, E_d, represents the dissipation of energy through molecular viscosity. On the neutral stability curve ($c_i = 0$), the disturbances are neither growing nor decaying, thus the left-hand-side term (differentiation with time) is zero.

3. Results and discussion

In addition to Re and Ra, the only other parameter in the system is Pr. A wide range of Pr was chosen in this study, starting with 0.7 for most gases, increasing to 7 for liquids, and reaching 100 for heavy oils. Because the stable and unstable domains are separated by the neutral stability curve ($c_i = 0$), we will basically present the neutral stability curves for fluids with various Pr to demonstrate the characteristics of stability for the flow. It is noted that $c_i = c_i(Re, Ra, \alpha, \beta)$ for all cases; therefore we will plot the neutral stability curves on both (Re, Ra)- and (Re, α)-planes for various typical β-values. We will also give the β-values that is associated with the least stable mode for most cases.

As mentioned previously, there are two ways to specify the temperature perturbations of the fluid at the boundaries. In the following we will present results first for the zero-temperature-perturbation case which corresponds to systems with thick highly conducting bounding walls. In their water experiment Scheele & Hanratty (1962) used highly conducting copper as the pipe wall material. The thermal conductivity of copper is three orders of magnitude larger than that of water. El-Genk & Rao (1990) employed a system where water is heated by stainless-steel tubing. It is therefore reasonable to assume that the case of zero temperature perturbation at the wall is a good approximation for the experimental system of both Scheele & Hanratty (1962) and El-Genk & Rao (1990). Since the motivation of this study is to attempt to explain the experimental observations of Scheele & Hanratty (1962) and El-Genk & Rao (1990), the following §§3.1 and 3.2 will be devoted to the discussion of results for the case of zero temperature perturbation on the boundaries. In §3.3, typical results for the zero heat flux perturbation will be presented and comparisons between the two different temperature perturbation boundary conditions will also be provided.

3.1. *Buoyancy-assisted flow*

First we examine the instability boundary for buoyancy-assisted flow on the (Re, Ra)-plane for $Pr = 7$, shown in the upper portion of figure 3(*a*). The flow instability boundaries are shown for spanwise wavenumbers $\beta = 0$, 1, 2 and 3. It should be pointed out that for the channel geometry there is no kinematic condition to require that β be an integer. Even though only curves for integer β-values are plotted we have included non-integer β-values in our computation for the determination of the β that is associated with the least-stable mode. The results suggest that a heated channel flow would become unstable for $Ra > 16.47$ and $Re > 40$. As a result, fully developed heated channel flow is extremely difficult to maintain even under a very mild heating condition. The critical Rayleigh number, Ra_c, is nearly constant (~ 15.7) for $Re > 100$,

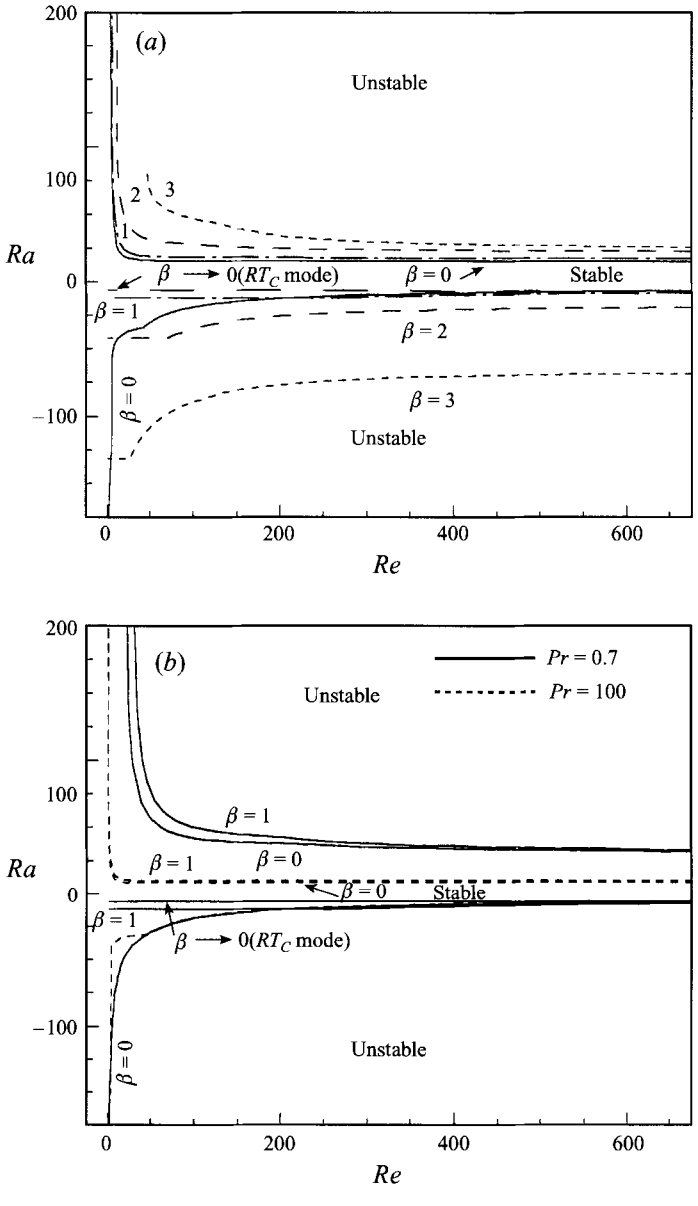

FIGURE 3. The instability boundaries on the (Re, Ra)-plane for (a) $Pr = 7$, (b) $Pr = 0.7$ and $Pr = 100$.

therefore there is no inflection point in the base flow because $Ra_c < 24.38$. But for very small Reynolds numbers (about 3.9–6.6) Ra_c goes through an almost vertical rise from 50 to 200. As pointed out by Yao (1987*a*), for stably stratified flow, slow convection flow is capable of bringing denser fluid upward into the region of lighter fluid, which explains our finding that heated flow becomes unstable even at very low velocities. The effect of the spanwise wavenumber, β, was also examined in figure 3(a) for both integer and non-integer values, where we found that $\beta = 0$ is the least-stable mode. The higher the value of β the more stable the mode. For $\beta \geqslant 5$, we were unable to find any unstable mode for $Pr = 7$. Next, the (Re, Ra)-plane for $Pr = 0.7$ and 100 is shown in figure 3(b).

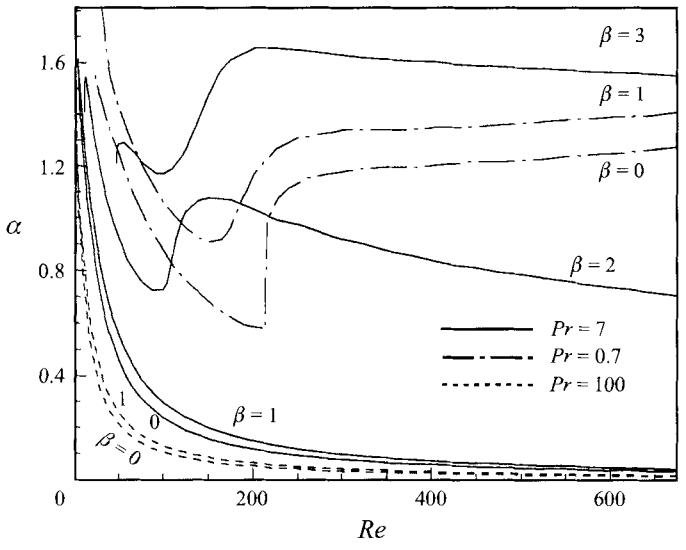

FIGURE 4. The variation of wavenumber α with Re along the neutral stability curve for buoyancy-assisted flows at $Pr = 0.7$, $Pr = 7$ and $Pr = 100$ ($\alpha_c = 1.0206$ for isothermal flow).

The $Pr = 100$ case is very close to that of $Pr = 7$ except that it is slightly more unstable for $Pr = 100$. The general trend for $Pr = 0.7$ is also similar to that of $Pr = 7$, but there is a fundamental difference between the two cases. The base laminar flow does contain inflection points in the $Pr = 0.7$ flows because Ra_c is greater than 24.38. This fundamental difference in the structure of the laminar base flow causes some drastically non-similar trends on the neutral stability curves on the (Re, α)-plane between $Pr = 0.7$ and $Pr = 7$ flows, which are shown in figure 4. Also, it is noted that $\beta = 0$ mode is the least stable for all three Prandtl number flows and therefore the least-stable disturbances are two-dimensional in the buoyancy-assisted case.

The linear instability boundary on the (α, Re) plane, where α is the wavenumber, for all three Prandtl numbers is plotted in figure 4. The curves demonstrate the variation of α with respect to Re_c along the neutrally stable curve. It is seen that for $\beta = 0$ and 1, α_c decreases monotonically with increasing Reynolds number for $Pr = 7$ and 100 and the effect of heating is quite dramatic as compared to the constant critical wavenumber of 1.0206 for isothermal channel flow. The wavelength of an unstable heated flow is shorter than that of an isothermal flow for high Ra and low Re while it is longer for flows with low Ra and high Re. Again, the difference between $\beta = 0$ and $\beta = 1$ is very small for $Pr = 7$ and 100. Furthermore, very similar trends are found between $Pr = 7$ and $Pr = 100$. For gases ($Pr = 0.7$), the critical wavenumber for $\beta = 0$ behaves in a similar manner to that for the liquid when the Reynolds number is less than about 215. Above this, instead of decreasing continuously with increasing Reynolds number as in the liquid case the critical wavenumber rises sharply and then quickly levels off to continue a slow climb. Therefore, for gases the unstable wavenumber is only slightly higher than that of an isothermal flow for $Re > 214$. We believe that this major difference in the neutrally stable wavenumber between liquids and gases for $Re > 214$ is because there is an inflection point in the base flow in these flows of gases but not in the $Pr = 7$ liquids. As shown in figures 3(*a*) and 3(*b*), the neutrally stable curve lies above the line of $Ra = 24.38$ for $Pr = 0.7$ but below it for $Pr = 7$ and $Re > 13$. Inflection points exist only in flows with $Ra \geqslant 24.38$.

Those entirely different trends on the (α, Re)-plane for $Pr = 0.7$ and $Pr = 7$ fluids for

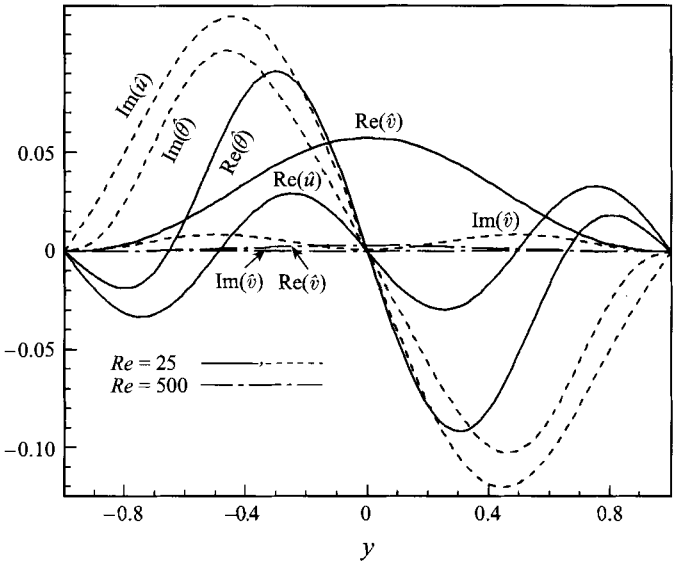

FIGURE 5. Eigenfunctions of $\hat{u}$, $\hat{v}$ and $\hat{\theta}$ on the neutral stability curve for $Pr = 7$ and $Re = 25$ and 500.

$Re > 150$ as shown in figure 4 could be further explained through the plots of eigenfunctions for $\hat{u}$, $\hat{v}$ and $\hat{\theta}$. Figure 5 presents these eigenfunction curves for $Pr = 7$ fluid at two different Reynolds numbers for $\beta = 0$. As mentioned above, the instability in the liquids ($Pr = 7$) is primarily due to the thermal buoyant force or heat transfer effects while velocity disturbances are more responsible for the instability in the gaseous fluids ($Pr = 0.7$). Rogers & Yao (1993*b*) also suggested that for larger-Prandtl-number fluids, the flow becomes unstable mainly due to the disruption of the velocity profile, induced by the temperature fluctuation. This difference in the causes of instability will be verified again in the disturbance energy budget analysis. As expected, the magnitudes of the temperature disturbance eigenfunctions are higher than those of the velocities for $Pr = 7$ fluid and generally the opposite holds for $Pr = 0.7$ fluids (not shown in figure 5).

We would like to suggest that there is a direct link between the value of α_c and the amplitude of the cross-stream disturbance $\hat{v}$ for $Pr = 7$ fluids. Based on figure 5, the amplitude of $\hat{v}$ is virtually zero for $Re = 500$ while the corresponding α_c is also vanishingly small at 0.048. This implies that for high-Reynolds-number flows, the least-stable disturbance is nearly one-dimensional in liquids ($Pr = 7$) and oils ($Pr = 100$). We could also come to this conclusion based on equation (10) ($i\alpha\hat{u} + i\beta\hat{w} + d\hat{v}/dy = 0$) for the disturbance continuity. In figure 5, at $Re = 25$ the diffusion mechanism dominates the convection for the low-Reynolds-number flow, which results in the increase of the amplitude of $\hat{v}$ to a finite quantity and accordingly the value of α_c to around 0.8. In fact we found that the value of α_c is directly proportional to the amplitude of $\hat{v}$ for $Pr = 7$ fluids.

Next the curves for various Reynolds numbers on the (c_i, α)-plane are shown in figure 6 for gaseous flows ($Pr = 0.7$). These curves should also shed some light on the special characteristics found on the (α, Re)-plane in figure 4 for $Pr = 0.7$ fluids. In figure 4, α_c dips to a minimum at $Re = 215$, therefore we plotted four curves in figure 6 for $Re = 190$, 210, 215 and 500. It is clear that the peak values of c_i associated with those curves on the (c_i, α)-plane are closely related to the special behaviour of the

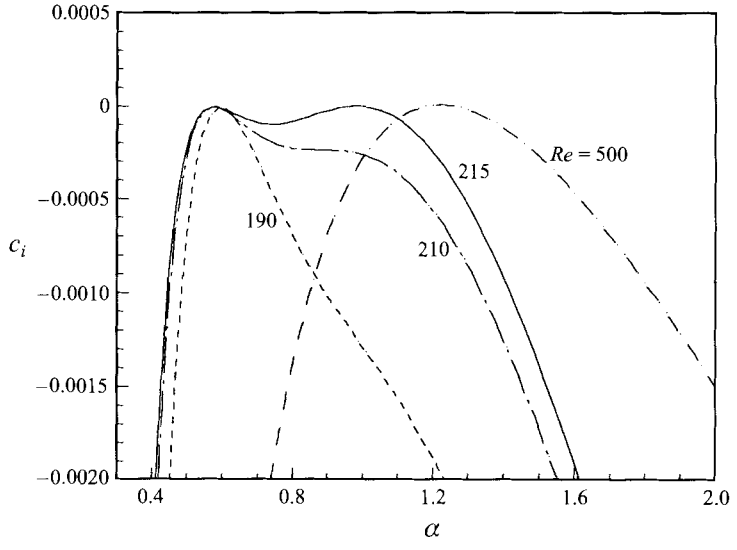

FIGURE 6. The variation of c_i with α for $Pr = 0.7$ at various Reynolds numbers.

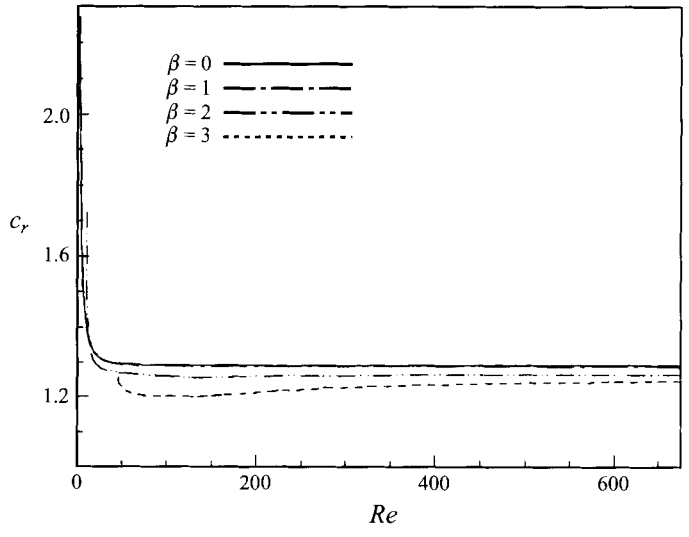

FIGURE 7. The variation of wave speed c_r with Re along the neutral stability curve for $Pr = 7$.

curves on the (α, Re)-plane. For $Re = 190$ and 500, each curve clearly has only a single peak and the α-locations for the peak c_i values correspond to the α-values on the (α, Re)-plane ($\alpha = 0.6$ for $Re = 190$ and $\alpha = 1.22$ for $Re = 500$). It is also quite reassuring that the curve for $Re = 210$ shows a tendency for the peak c_i position to move gradually from the lower-α to the higher-α region. For the $Re = 215$ case, where the vertical rise takes place on the (α, Re)-plane, we found that the α-locations of the two c_i peaks correspond exactly to the lowest α-value (~ 0.58) and the highest α-value (~ 0.98) on the vertical line at $Re = 215$ in figure 4. It is clear that there is a direct relationship between the peak value of c_i on the (c_i, α)-plane and the trend of the neutrally stable curve on the (Re, α)-plane.

The wave speed, c_r, along the instability boundary is plotted for $Pr = 7$ in figure 7

Pr	Re	Ra_c	α_c	E_s	E_b	E_d	Type
100	100	8.61	0.108	−0.06	1.06	−1.0	TB
100	500	8.6	0.022	−0.06	1.06	−1.0	TB
100	1000	8.6	0.011	−0.06	1.06	−1.0	TB
7	3.97	500	1.64	−0.05	1.05	−1.0	TB
7	100	15.73	0.24	−0.14	1.14	−1.0	TB
7	500	15.60	0.048	−0.145	1.145	−1.0	TB
7	1000	15.60	0.024	−0.145	1.145	−1.0	TB
7	3848.147	0.0	1.020 56	1.00	0.00	−1.0	S
0.7	28.34	500	1.46	0.40	0.60	−1.0	M
0.7	30	96.93	1.465	0.30	0.70	−1.0	M
0.7	100	41.65	0.875	0.075	0.925	−1.0	TB
0.7	140	39.21	0.715	0.05	0.95	−1.0	TB
0.7	214	37.61	0.577	0.03	0.97	−1.0	TB
0.7	215	37.60	0.98	0.08	0.92	−1.0	TB
0.7	500	32.65	1.22	0.07	0.93	−1.0	TB
0.7	1000	30.26	1.355	0.06	0.94	−1.0	TB

TABLE 1. Energy budget for the neutral stability curve for buoyancy-assisted flow (TB: thermal–buoyant instability; TS: thermal–shear instability; M: mixed instability; S: shear instability).

for $\beta = 0$, 1, 2 and 3. Essentially, the wave speed of the dominant mode $\beta = 0$ is constant at about 1.3 for $Re > 30$. The waves travel much faster at low Reynolds numbers. Because of close similarity, the wave speed curves for $Pr = 0.7$ and 100 are not shown here.

As mentioned earlier, the analysis of the energy transfer budget for the neutral stability curve could provide some insight into the transport mechanisms during flow instability. A summary of the energy budget for buoyancy-assisted flows is given in table 1. As mentioned previously for heated confined flows, Rogers & Yao (1993*b*) have identified thermal–shear and thermal–buoyant as the major thermal instabilities. Unlike the annulus flow, where the thermal–shear instability prevails for $Pr = 1$ and the thermal–buoyant instability dominates for $Pr = 6$ and 100, we found that the thermal–buoyant instability is the only mode for Prandtl numbers ranging from 0.7 to 100 in buoyancy-assisted channel flow. Therefore, only for gases, the thermal instability types are significantly different for annulus and channel geometries. Another important finding is the identification of a mixed mode of instability between the thermal–shear and thermal–buoyant instability for flows with $Pr = 0.7$ and relatively low Reynolds numbers which correspond to the almost vertical portion of the neutral stability curve on the (Re, Ra)-plane. This mixed mode initially obtains its energy roughly evenly from both shear and buoyant sources. Also it is worth noting that most E_s values for $Pr = 7$ fluids are negative and we attribute that to the lack of an inflection point in the base flow. E_s is positive for all $Pr = 0.7$ fluids, where an inflection point is found in every one of them.

3.2. *Buoyancy-opposed flow*

The neutral stability curves on the (Re, Ra)-plane for buoyancy-opposed flow at $Pr = 7$ are plotted in the lower portion of figure 3 (*a*). We found that for $Re < 641$ the least-stable mode for buoyancy-opposed flow belongs to the Rayleigh–Taylor instability. We call this least-stable instability a critical Rayleigh–Taylor mode and use the symbol RT_C to represent it. It will be verified later that the RT_C mode is indeed the Rayleigh–Taylor-type instability. The characteristics of the RT_C mode are that the

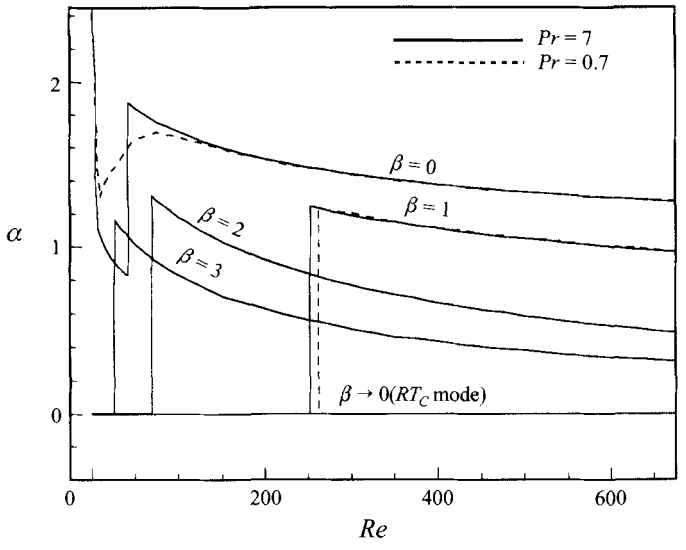

FIGURE 8. The variation of wavenumber α with Re along the neutral stability curve for buoyancy-opposed flows at $Pr = 0.7$ and $Pr = 7$ ($\alpha_c = 1.0206$ for isothermal flow).

streamwise wavenumber, α, asymptotically approaches zero while the corresponding spanwise wavenumber, β, is also vanishingly small. For the RT_C mode, the critical Rayleigh number, Ra_c, and the wave speed are -6.1 and 1.35, respectively. Note that the RT_C mode is different from the $\beta = 0$ mode which is a thermal–shear instability with a finite streamwise wavenumber around 1.5. The Rayleigh–Taylor instability with streamwise wavenumber asymptotically approaching zero has also been found as the least-stable mode for low-Reynolds-number mixed-convection flow in a vertical annulus (Rogers & Yao 1993*b*). For $Re > 641$, the two-dimensional disturbance ($\beta = 0$) mode with a finite value of α becomes the least-stable mode where the $|Ra_c|$ decreases slightly with increasing Re_c. Therefore the least-stable mode for $Re < 641$ in buoyancy-opposed flow is not two-dimensional, while it is two-dimensional with a finite non-zero streamwise wavenumber in buoyancy-assisted flow. We also plotted $\beta = 1$, 2, 3 curves. Again, for $\beta > 1$ the disturbance waves are always more stable. The instability boundaries on the (Re, Ra)-plane for $Pr = 0.7$ and $Pr = 100$ are shown in the lower half of figure 3(*b*) where we found very similar trends to those for $Pr = 7$. It is noted that Ra_c and the wave speed for $Pr = 0.7$ and 100 also remain the same as for $Pr = 7$ for the RT_C mode. It is reasonable to suggest that the instability boundaries on the (Re, Ra)-plane are less dependent on the Prandtl number for most gases, liquids and heavy oils. For relatively low Reynolds numbers, $Re < 654$ for $Pr = 0.7$ and $Re < 594$ for $Pr = 100$, as shown in table 2, the instability is dominated by the Rayleigh–Taylor mode and independent of the fluid type.

The instability boundaries on the (Re, α)-plane are plotted in figure 8 for $Pr = 0.7$ and 7. Very similar trends are found for the two cases. We do not show the $Pr = 100$ case because it is also very similar to the $Pr = 7$ case. Recall that the instability boundaries on the (Re, α)-plane for the same Prandtl numbers of 0.7 and 7 but under the buoyancy-assisted flow condition are distinctively different (figure 4). This implies that the Prandtl number has a much smaller effect on α_c in the buoyancy-opposed flow. Figure 8 also shows that α_c has a jump at $Re \sim 42$ for the $\beta = 0$ mode. On both sides of the jump, α_c decreases with increasing Re; it is larger than that of the isothermal flow for $Re > 42$. It is noted that the trend of a sudden jump of α_c for all Prandtl numbers

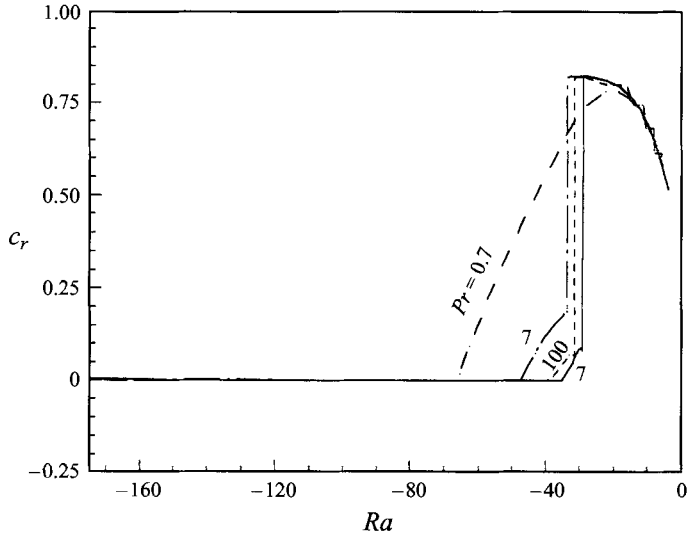

FIGURE 9. The variation of wave speed c_r with Ra along the neutral stability curve for $\beta = 0$ at various Prandtl numbers (solid line is associated with the zero heat flux perturbation boundary condition for $Pr = 7$).

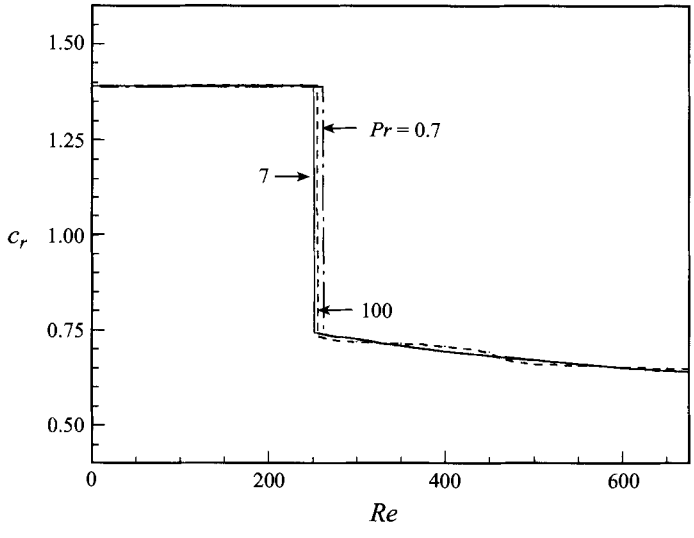

FIGURE 10. The variation of wave speed c_r with Re along the neutral stability curve for $\beta = 1$ at various Prandtl numbers.

in buoyancy-opposed flow is only found for $Pr = 0.7$ in buoyancy-assisted flow (figure 4). Also, after the jump, α_c increases with Re in buoyancy-assisted flow. As shown in figure 8, the difference between the $\beta = 0$ mode and the RT_C mode is clearly demonstrated on the (Re, α)-plane in terms of the magnitude of the streamwise wavenumber. For $\beta = 1$, 2 and 3, the critical wavenumbers all show similar trends and the Reynolds number at which the critical wavenumber experiences a jump decreases with increasing β-value.

The instability boundaries on the (Ra, c_r)-plane are given for $\beta = 0$ in figure 9 and

Pr	Re	Ra_c	α_c	E_s	E_b	E_d	Type
100	50	−6.10	0.00	0.00	1.00	−1.0	RT
100	500	−6.10	0.00	0.00	1.00	−1.0	RT
100	625	−6.00	1.356	0.85	0.15	−1.0	TS
100	1000	−4.24	1.238	0.90	0.10	−1.0	TS
100	1750	−2.49	1.137	0.95	0.05	−1.0	TS
100	2500	−1.71	1.062	0.98	0.02	−1.0	TS
7	50	−6.10	0.00	0.00	1.00	−1.0	RT
7	500	−6.10	0.00	0.00	1.00	−1.0	RT
7	650	−6.04	1.276	0.87	0.13	−1.0	TS
7	1000	−4.54	1.20	0.92	0.08	−1.0	TS
7	1750	−2.72	1.11	0.96	0.04	−1.0	TS
7	2500	−1.54	1.065	0.98	0.02	−1.0	TS
7	3848.147	−0.0	1.020 56	1.00	0.00	−1.0	S
0.7	50	−6.10	0.00	0.00	1.00	−1.0	RT
0.7	600	−6.10	0.00	0.00	1.00	−1.0	RT
0.7	660	−6.06	1.275	0.88	0.12	−1.0	TS
0.7	1000	−4.58	1.20	0.92	0.08	−1.0	TS
0.7	1750	−2.74	1.11	0.96	0.04	−1.0	TS
0.7	2500	−1.54	1.065	0.98	0.02	−1.0	TS

TABLE 2. Energy budget for the neutral stability curve for buoyancy-opposed flow (RT: Rayleigh–Taylor instability; TS: thermal–shear instability; S: shear instability).

on the (Re, c_r) plane for $\beta = 1$ in figure 10. We have covered a wide range of Prandtl numbers ($Pr = 0.7$, 7 and 100) and it is apparent that the Prandtl-number dependence is relatively minor. On the (Ra, c_r)-plane in figure 9, the important finding is that c_{r_c} stays very close to zero for increasing $|Ra|$ and there is a sudden rise at $Ra \sim -40$. For $0 < |Ra| \leqslant 40$, c_{r_c} varies between 0.6 and 0.8. In figure 10, there are two distinctive regions on the (Re, c_r)-plane. The abrupt transition takes place at $Re = 257$ for water and at $Re = 263$ for air. For the lower-Re portion, c_{r_c} stays around 1.38 and it decreases slowly from 0.75 to 0.65 for the higher-Re portion.

A summary of the energy budget analysis for buoyancy-opposed flow is given in table 2. There are major differences between buoyancy-assisted and buoyancy-opposed channel flows in the energy budget analysis. Either the Rayleigh–Taylor instability or the thermal–shear instability dominates in buoyancy-opposed flows whereas the thermal–buoyant instability is the dominant type in buoyancy-assisted flows. In general for Prandtl numbers ranging from 0.7 to 100 in buoyancy-opposed flow, we found that the Rayleigh–Taylor instability prevails for low-Re flows, where the energy for the disturbances comes solely from the buoyant potential and none from the shear production ($E_b = 1.0$ and $E_s = 0$). The instability is thermal–shear for higher Reynolds numbers and the energy contribution from buoyancy production decreases with increasing Reynolds number. It is noted that the instability is still classified as thermal–shear instability for $Re = 2500$, even though the buoyant energy contribution is only 2% or less. These are thermal–shear instabilities rather than shear instabilities because the corresponding isothermal flows are linearly stable ($Re_c = 3848.1$ for isothermal flow, based on mean velocity). Compared to the instability in mixed-convection annulus flow, Rogers & Yao (1993*b*) found that the thermal–buoyant instability prevails at $Pr = 100$ for the low-Re flow and the fraction of energy contribution from the buoyancy production is very small at higher Reynolds numbers. Again the Prandtl number does not have a visible effect on the relationship between Re and the dominant instability type. We may also conclude that the instability in

		Buoyancy-assisted				Buoyancy-opposed			
Pr	Re	Ra	α	β	$(\alpha c_i)_{max}$	Ra	α	β	$(\alpha c_i)_{max}$
7	800	100	2.50	0	0.17907	−100	2.06	0	1.50601
7	800	100	2.40	1	0.16299	−100	1.96	1	1.32510
7	800	100	2.14	2	0.11642	−100	1.62	2	0.81155
7	800	100	1.66	3	0.04894	−100	0.92	3	0.14076
0.7	800	100	2.48	0	0.17976	−100	2.06	0	1.50602
0.7	800	100	2.40	1	0.16360	−100	1.96	1	1.32511
0.7	800	100	2.12	2	0.11673	−100	1.62	2	0.81159
0.7	800	100	1.62	3	0.04870	−100	0.90	3	0.14061
100	800	100	2.50	0	0.17961	−100	2.06	0	1.50602
100	800	100	2.42	1	0.16379	−100	1.96	1	1.32511
100	800	100	2.16	2	0.11696	−100	1.62	2	0.81153
7	1200	100	2.48	0	0.18636	−100	2.06	0	1.52127
7	1200	100	2.40	1	0.17021	−100	1.96	1	1.33992
7	1200	100	2.12	2	0.12325	−100	1.62	2	0.82444
7	800	200	2.14	0	0.32643	−200	2.40	0	10.87535
7	800	200	2.04	1	0.29063	−200	2.28	1	9.92040
7	800	200	1.76	2	0.19329	−200	1.98	2	7.11070
7	800	200	1.24	3	0.07400	−200	1.42	3	2.93097

TABLE 3. The maximum amplification rate for various β values for buoyancy-assisted and buoyancy-opposed flows.

buoyancy-opposed flow is less sensitive to the thermal effects as either the Rayleigh–Taylor or thermal–shear instability dominates. In buoyancy-assisted flows, the instability is more sensitive to the heat transfer because the thermal–buoyant instability dominates.

As reviewed earlier, Scheele & Hanratty (1962) reported that there is a distinctive difference in the transition phenomena between buoyancy-assisted and buoyancy-opposed pipe flows. Transition to turbulence proceeds gradually in a finite downstream distance for buoyancy-assisted flow while it is a sudden and abrupt process in buoyancy-opposed flow. Similar phenomena were observed in heated vertical annulus flows by El-Genk & Rao (1990). There is no experimental report concerning the transition behaviour in heated channel flows. Because of the many similarities between pipe and channel flows, we expect different transition patterns for buoyancy-assisted and buoyancy-opposed channel flows. Even though linear stability theory is only relevant to the onset of the instability and transition process, we would like to offer some suggestions for the causes for the observed different transition behaviours. As shown before for buoyancy-opposed flow, we found that the wave speed, c_r, is diminishingly small for $|Ra| \geqslant 40$ in heavy oils, $|Ra| \geqslant 48$ in water and $|Ra| > 70$ in air, while c_r is about 1.29 for buoyancy-assisted flow. As pointed out by Gaster (1962), the relationship between the temporal and spatial instabilities may be correlated by exchanging the roles of the streamwise coordinate x and the time t as $x \propto c_r t$. Since c_r is vanishingly small, the spatial development distance for the disturbance is accordingly very short for buoyancy-opposed flow, whereas a finite distance is expected for buoyancy-assisted flow due to the finite value of 1.29 for c_r. Further supporting evidence comes from the disturbance amplification rates. Table 3 lists the maximum amplification rates for typical cases of both buoyancy-assisted and buoyancy-opposed flows. It is apparent that the amplification rates for buoyancy-opposed flow are one to two orders of magnitude higher than those for buoyancy-assisted flow. This difference

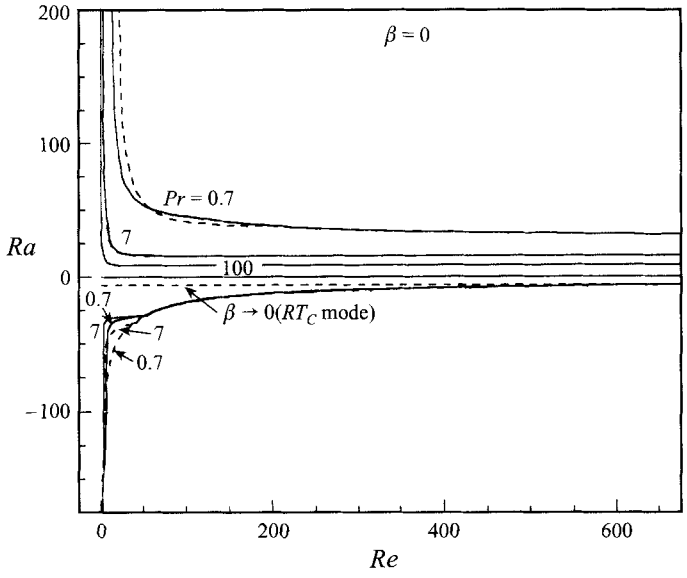

FIGURE 11. The instability boundaries on the (Re, Ra)-plane for the zero heat flux perturbation boundary condition. (Dashed lines show zero temperature perturbation condition from figure 3).

in the amplification rates provides further support for the two distinctive flow transition patterns. The results in table 3 also indicate that $\beta = 0$ is the dominant mode in those flows.

3.3. *Zero heat flux perturbation boundary condition*

3.3.1. *Buoyancy-assisted flows*

In this section, we present typical results for the case where the derivatives of temperature perturbation with respect to y at the boundaries are zero but the temperature perturbation remains non-zero. For the convenience of discussion, we call the zero temperature perturbation boundary condition case A and the zero heat flux perturbation case B. First the neutral stability curves for the least-stable ($\beta = 0$) mode buoyancy-assisted flow on the (Re, Ra)-plane are plotted in the upper portion of figure 11 as solid lines for case B. For comparison, some results presented before in figure 3 for case A are repeated as dashed lines in figure 11. The differences between cases A and B are most pronounced for the $Pr = 0.7$ flow. For $Re > 410$ there is virtually no difference. Case B is slightly more unstable for Re in the range of 215 to 410 while case A is more unstable in the range of 63 to 215 where the corresponding wavenumber is minimum. For $Ra > 50$ and $Re < 63$, case B is again more unstable. For $Pr = 7$, there is no difference for $Re > 100$. Case A is slightly more unstable for Re in the range of 7.5 to 100. Case B becomes more unstable for $Ra > 75$. For $Pr = 100$, essentially there is no difference between the two cases for $Re > 2$. This is as expected, since the momentum diffusivity is much larger than the thermal diffusivity for $Pr = 100$ fluids. In summary, for buoyancy-assisted flows, the differences in stability characteristics between the two types of temperature perturbation boundary condition are inversely proportional to both Re and Pr. The stability boundaries on the (Re, α)-plane for the $\beta = 0$ mode are plotted in figure 12. Again we have repeated the corresponding results with zero temperature perturbation boundary condition as dashed lines. The differences in streamwise wavenumber between cases A and B are very minor for $Pr = 7$ and 100. For $Pr = 0.7$, the basic trends are similar but local minima of the wavenumbers are located at different Reynolds numbers. The minimum wavenumber α_c occurs at $Re =$

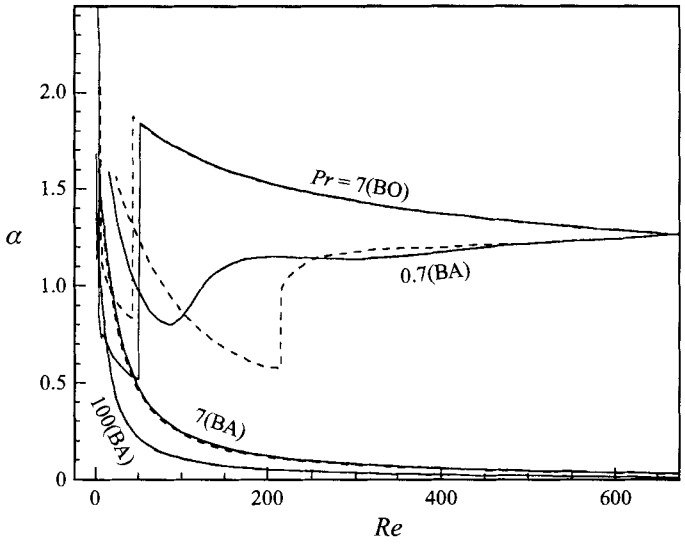

FIGURE 12. The variation of wavenumber α with Re along the neutral stability curve for the zero heat flux boundary condition (BA: Buoyancy-assisted flow; BO: Buoyancy-opposed flow). Dashed lines show zero temperature perturbation condition.

214 with a value of 0.58 for case A while it occurs at the Reynolds number of about 87 with a value of 0.8 for case B. Similarly to the (Ra, Re)-plane comparison, the differences between cases A and B on the (α, Re)-plane diminish for higher Reynolds numbers. We also calculated the maximum amplification rates for case B and compared them with those of case A listed in table 3. It is found that the maximum amplification rates associated with case B agree with those in table 3 to the fourth decimal point. From the above discussion, we may conclude that the condition of zero heat flux perturbation at the walls produces very limited changes to the stability characteristics from those with zero temperature perturbation for buoyancy-assisted flow except for $Pr = 0.7$ fluid at low Reynolds numbers.

3.3.2. *Buoyancy-opposed flows*

For buoyancy-opposed flow, the neutral stability curves on the (Re, Ra)-plane for $Pr = 0.7$ and 7 are shown in the lower half of figure 11. Again the dashed and solid lines represent cases A and B respectively. First we discuss the $\beta = 0$ mode where the streamwise wavenumbers remain finite. For $Pr = 7$, there is essentially no difference between cases A and B for $Re > 70$. Case B is slightly more unstable for Reynolds numbers less than 70. For $Pr = 0.7$, again there is no difference for $Re > 70$. Case B is more unstable for the Reynolds number in the range of 8 to 70. Case A becomes slightly more unstable when $|Ra|$ is greater than 100. We also plotted the $\beta = 0$ neutral stability boundaries on the (Re, α)-plane for $Pr = 7$ in figure 12. It is consistent with the (Ra, Re)-plot in that the difference is significant only for $Re < 70$. It is reasonable to conclude that the effects of the temperature perturbation at the walls for buoyancy-opposed flows are also limited to lower Reynolds numbers for the $\beta = 0$ mode. The major difference which is also of practical importance between cases A and B for buoyancy-opposed flow is associated with the Rayleigh–Taylor mode of instability. Recall that the main characteristic of this mode is that the streamwise wavenumber is approaching zero while β is also vanishingly small. The critical Rayleigh number, Ra_c, shown in figure 11 for the RT_C mode also was found to approach zero for case B, while

it is finite at -6.10 for case A. This result is independent of the Prandtl number. In other words, for case B, buoyancy-opposed flow tends to be unstable for any Reynolds number because the critical Rayleigh number is approach zero. It is therefore significant to note that the only way to maintain a stable buoyancy-opposed flow with a constant heat flux at the boundary is to use highly conducting materials for bounding walls such that case A can be simulated. The wave speeds and the maximum amplification rates, which are important in explaining the different transition patterns between buoyancy-assisted and -opposed flows, are also computed for case B. The solid line in figure 9 is the wave speed for case B and $Pr = 7$. The wave speed also becomes very small for $|Ra| > 32.2$. The maximum amplification rates associated with case B were found to agree with those of case A listed in table 4 to third decimal point. Thus the differences caused by the zero heat flux perturbation at the walls have a rather minor effect on the instability characteristics for the $\beta = 0$ mode whereas they are relatively significant for the Rayleigh–Taylor mode. The zero heat flux perturbation produces no major changes in wave speeds and maximum amplification rates.

4. Conclusions

The linear stability analysis of mixed convection in a vertical channel with constant heat flux imposed on the walls was investigated for two different temperature perturbations at the boundaries. For the first case where the bounding walls are made of highly conducting materials, zero temperature perturbation was assumed at the boundaries; zero heat flux perturbation at the boundaries was assumed for the second case. The results in general indicate that the fully developed heated flow is very unstable and therefore very difficult to find in nature.

For the case of zero temperature perturbation at the walls, heated water flow ($Pr = 7$) can become unstable if $Ra > 16.47$ and $Re > 40$ for buoyancy-assisted flows and $|Ra| > 6.1$ for buoyancy-opposed flows. The results also show that the two-dimensional disturbance with a zero spanwise wavenumber and a finite streamwise wavenumber is the most unstable wave in buoyancy-assisted flow. The critical wavenumber shows a distinctively different behaviour between the liquids ($Pr = 7$ and 100) and the gases ($Pr = 0.7$): the wavenumbers of liquids are very small for $Re > 100$ (for $Pr = 7$, $\alpha_c = 0.048$ at $Re = 500$ and $\alpha_c = 0.024$ at $Re = 1000$) and that of air is slightly larger than that of the isothermal flow ($\alpha_c = 1.02056$) for $Re > 215$ in buoyancy-assisted flow. This means that the most unstable disturbance is nearly one-dimensional for $Pr = 7$ and 100 at high Reynolds numbers. The energy budget analysis for buoyancy-assisted flow indicates that the dominant instabilities for air ($Pr = 0.7$), water ($Pr = 7$) and oil ($Pr = 100$) all belong to the thermal–buoyant instability.

Additionally, the linear stability results for buoyancy-opposed flows under zero temperature perturbations at the walls show that for $Re < 594$–654 the most unstable wave was found to be the Rayleigh–Taylor instability with the streamwise wavenumber asymptotically approaching zero and the corresponding spanwise wavenumber is also vanishingly small. The corresponding critical Rayleigh number and wave speed are -6.10 and 1.35, respectively. The critical streamwise wavenumbers for both water and air show very similar behaviour in buoyancy-opposed flow, although they have distinctly different behaviour in buoyancy-assisted flow. The curves of the critical wavenumber for $\beta = 0$, 1, 2 and 3 abruptly change at certain Reynolds numbers. Because the instability characteristics found for $Pr = 0.7$, 7 and 100 are all similar, it may be concluded that the Prandtl number has little effect on buoyancy-opposed flow instability. When the absolute value of the critical Rayleigh number is greater than a

certain value between 40 and 70, the wave speed of the instability approaches zero for the two-dimensional disturbance ($\beta = 0$). Based on the relationship of the temporally increasing and spatially increasing disturbances (by exchanging the roles of the streamwise coordinate and the time), we found that the required distance for the disturbance development in buoyancy-opposed flow is much shorter than that of buoyancy-assisted flow, which might help explain why buoyancy-opposed flows go through transition suddenly and buoyancy-assisted flows go through transition gradually. That the disturbance amplification rates of buoyancy-opposed flow are generally one to two orders of magnitude higher than those of buoyancy-assisted flow provides further support for the different transition patterns. The energy budget analysis for buoyancy-opposed flow shows that the instability for lower Reynolds number flows in air, water and heavy oil is of the Rayleigh–Taylor type. For higher Reynolds numbers, the dominant instability switches to the thermal–shear instability and the energy contribution from buoyancy production decreases with increasing Reynolds number.

The instability characteristics of zero heat flux perturbations on the boundaries are in general very similar to those of the zero temperature perturbation case for buoyancy-assisted flows. The two cases are practically identical for higher Reynolds numbers. At lower Reynolds numbers, only minor differences were found and the differences decrease with increasing Prandtl number. For buoyancy-opposed flow, the differences are minor for the thermal–shear mode of instability between the two cases. Major differences were found for the Rayleigh–Taylor instability. The critical Rayleigh number is -6.10 for zero temperature perturbation while it is approaching zero for zero heat flux perturbation. The maximum amplification rates were found insensitive to the different temperature perturbations on the boundaries for both assisted and opposed flows.

The comments and suggestions from the reviewers are very much appreciated. The National Center for Supercomputing Applications (NCSA) at the Illinois provided the computing resources to this research.

REFERENCES

BUSSE, F. H. 1981 Transition to turbulence in Rayleigh–Benard convection. In *Hydrodynamic Instabilities and Transition to Turbulence* (ed. H. L. Swinney & J. P. Gollub), chap. 5. Springer.

DAVIS, P. J. & RABINOWITZ, P. 1984 *Methods of Numerical Integration*. Academic Press.

DRAZIN, P. G. & REID, W. H. 1981 *Hydrodynamic Stability*. Cambridge University Press.

EL-GENK, M. S. & RAO, D. V. 1990 Buoyancy induced instability of laminar flows in vertical annuli-I. flow visualization and heat transfer experiments. *Intl J. Heat Mass Transfer* **33**, 2145–2159.

GASTER, M. 1962 A note on the relation between temporally-increasing and spatially-increasing disturbances in hydrodynamic stability. *J. Fluid Mech.* **14**, 222–224.

GEBHART, B., JALURIA, Y., MAHAJAN, R. L. & SAMMAKIA, B. 1988 *Buoyancy-Induced Flows and Transport*. Hemisphere.

HANRATTY, T. J., ROSEN, E. M. & KABEL, R. L. 1958 Effect of heat transfer on the flow field at low Reynolds numbers in vertical tubes. *Ind. Engng Chem.* **50**, 815–820.

HART, J. E. 1971 Stability of the flow in a differentially heated inclined box. *J. Fluid Mech.* **47**, 547–576.

KEMENY, G. A. & SOMERS, E. V. 1962 Combined free and forced convection in vertical circular tubes – experiments with water and oil. *Trans. ASME* C: *J. Heat Transfer* **108**, 339–346.

MAITRA, D. & RAJU, K. S. 1975 Combined free and forced convection laminar heat transfer in a vertical annulus. *Trans. ASME* C: *J. Heat Transfer* **97**, 135–137.

ORSZAG, S. A. 1971 Accurate solution of the Orr–Sommerfeld stability equation. *J. Fluid Mech.* **50**, 689–703.

OSTRACH, S. 1954 Combined natural and forced-convection laminar flow and heat transfer of fluids with and without heat sources in channels with linearly varying wall temperatures. *NACA TN* 3141.

ROGERS, B. B., MOULIC, S. G. & YAO, L. S. 1993 Finite-amplitude instability of mixed convection. *J. Fluid Mech.* **254**, 229–250.

ROGERS, B. B. & YAO, L. S. 1993*a* Finite-amplitude instability mixed-convection in a heated vertical pipe. *Intl J. Heat Mass Transfer* **36**, 2305–2315.

ROGERS, B. B. & YAO, L. S. 1993*b* The importance of Prandtl number in mixed-convection instability. *Trans. ASME* C: *J. Heat Transfer* **115**, 482–486.

SCHEELE, G. F. & HANRATTY, T. J. 1962 Effect of natural convection on stability of flow in a vertical pipe. *J. Fluid Mech.* **140**, 244–256.

SCHEELE, G. F., ROSEN, E. M. & HANRATTY, T. J. 1960 Effect of natural convection on transition to turbulence in vertical pipes. *Can J. Chem. Engng* **38**, 67–73.

SINGER, B. A., FERZIGER, J. H. & READ, H. L. 1989 Numerical simulations of transition in oscillatory plane channel flow. *J. Fluid Mech.* **208**, 45–66.

SPARROW, E. M., GOLDSTEIN, R. J. & JONSSON, V. K. 1964 Thermal instability in a horizontal fluid layer: effect of boundary conditions and non-linear temperature profile. *J. Fluid Mech.* **18**, 513–528.

TAO, L. N. 1960 On combined free and forced convection in channel. *Trans. ASME* C: *J. Heat Transfer* **82**, 233–238.

YAO, L. S. 1987*a* Is fully developed and non-isothermal flow possible in a vertical pipe? *Intl J. Heat Mass Transfer* **30**, 707–715.

YAO, L. S. 1987*b* Linear Stability analysis for opposing mixed convection in a vertical pipe. *Intl J. Heat Mass Transfer* **30**, 810–811.

YAO, L. S. & ROGERS, B. B. 1989*a* The linear stability of mixed convection in a vertical annulus. *J. Fluid Mech.* **201**, 279–298.

YAO, L. S. & ROGERS, B. B. 1989*b* Mixed convection in a annulus of large aspect ratio. *Trans. ASME* C: *J. Heat Transfer* **111**, 683–689.

YAO, L. S. & ROGERS, B. B. 1992 Finite-amplitude instability of non-isothermal flow in a vertical annulus. *Proc. R. Soc. Lond.* A **437**, 267–290.